Available online at www.sciencedirect.com

ScienceDirect

journal homepage: www.elsevier.com/locate/he

Obtaining particles with the structure Mg@C and (Mg@C)@Pd, their properties and stability in the hydrogenation/dehydrogenation processes

G.N. Churilov [a,b], N.S. Nikolaev [a,b,*], V.I. Elesina [a,b], G.A. Glushenko [b], V.G. Isakova [b], Ye.V. Tomashevich [c]

[a] Institute of Engineering Physics and Radio Electronics, Siberian Federal University, Svobodny, 79, Krasnoyarsk, 660041, Russia

[b] Kirensky Institute of Physics, Federal Research Center KSC SB RAS, Akademgorodok 50/38, Krasnoyarsk, 660036 Russia

[c] Institute of Chemistry and Chemical Technology, Federal Research Center KSC SB RAS, Akademgorodok 50/24, Krasnoyarsk, 660036 Russia

HIGHLIGHTS

- A technique has been developed to obtain particles with the (Mg@C)@Pd structure.
- Shown that (Mg@C)@Pd particles have a high sorption capacity ofhydrogen 6.95 wt.%.
- The accumulation of MgO and $Mg(OH)_2$ decreases a hydro-genationrecycle stable.
- The large particles (Mg@C)@Pd is less stable than the small ones.

GRAPHICAL ABSTRACT

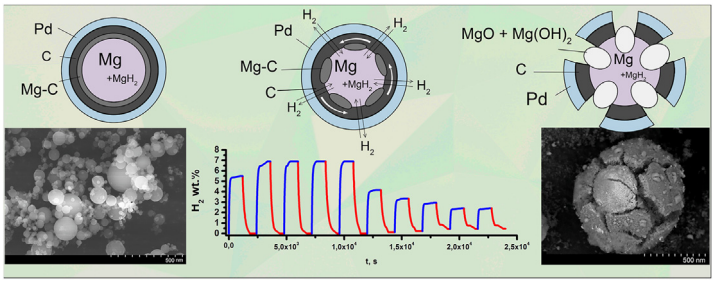

ARTICLE INFO

Article history:
Received 29 June 2020
Received in revised form
5 March 2021
Accepted 7 March 2021
Available online xxx

Keywords:
Core-shell particles
Mg, C, Pd nanoparticles
Sorption capacity of hydrogen

ABSTRACT

In this work, we studied the change in the properties of powders with a core (magnesium) – shell structure (carbon and carbon/palladium) in the process of hydrogenation/dehydrogenation with hydrogen (99.995 wt%). Magnesium powders were obtained by plasma chemical synthesis in an atmosphere of argon containing a small amount of hydrogen (2–3 at.%) and nitrogen (8–9 at.%), when performing a low-frequency arc discharge between a tungsten electrode and a magnesium melt. The shell (carbon and carbon/palladium) was deposited in a plasma generator with vortex and magnetic stabilization. For all samples, a decrease in the sorption capacity of hydrogen was observed as a result of successive cycles of sorption and desorption reactions. It was found that the reason for this fall is associated with the formation of the MgO and $Mg(OH)_2$ phase, which prevents the diffusion of hydrogen. The carbon shell provides a more complete hydrogenation of the magnesium

* *Corresponding author*. Kirensky Institute of Physics, Federal Research Center KSC SB RAS, Akademgorodok 50/38, Krasnoyarsk, 660036, Russia.
E-mail addresses: a6rukoc@yandex.ru, xnaodurb@gmail.ru (N.S. Nikolaev).

https://doi.org/10.1016/j.ijhydene.2021.03.042

0360-3199/© 2021 Hydrogen Energy Publications LLC. Published by Elsevier Ltd. All rights reserved.

Please cite this article as: Churilov GN et al., Obtaining particles with the structure Mg@C and (Mg@C)@Pd, their properties and stability in the hydrogenation/dehydrogenation processes, International Journal of Hydrogen Energy, https://doi.org/10.1016/j.ijhydene.2021.03.042

Hydrogen-storage materials
Magnesium hydride

particles, and an additional palladium shell increases the resistance to cyclic hydrogenation/dehydrogenation and reduces the temperature of these processes. According to the data obtained, powders with particles (Mg@C)@Pd can absorb the largest amount of hydrogen (6.9 wt%) for the duration of 5 cycles, after which the protective shell of the particles begins to collapse and a loss of sorption capacity is observed.

© 2021 Hydrogen Energy Publications LLC. Published by Elsevier Ltd. All rights reserved.

Introduction

The need to obtain new materials and methods for storing energy is a strategic task. Hydrogen is now considered an important energy source for the future. However, storage of hydrogen is challenging. There are still significant problems that need to be solved for its use as a fuel. Among these challenges, the development of a new technology for the safe storage of hydrogen with high bulk and gravimetric density and without the use of a heating system is the key.

Modern hydrogen storage methods include:

- gaseous storage under high pressure (350–700 bar at room temperature), which is not advisable due to the large volume and low energy efficiency;
- cryogenic liquid storage (−253 °C, 5–10 bar) as it requires special and expensive tanks to ensure reliable and safe storage of hydrogen;
- solid state storage [1–3].

Solid-state hydrogen storage has a range of advantages: high gravimetric and volumetric densities of stored hydrogen, moderate operating pressures, and high energy efficiency [4–6]. Over the past decades, various types of materials for hydrogen storage have been discovered and studied [7,8], among them both adsorbents and absorbents are known [9,10]. The latter have recently received massive attention [11].

One of the methods for safe storage of high-density hydrogen is the use of different hydrides.

Among all the materials studied for hydrogen storage, the MgH2 hydrogen solid state storage is quite promising. It has a high gravimetric hydrogen capacity. The gravimetric hydrogen capacity is 7.6 wt% [4] by weight and 110 kg/m^3 in volume. It is also characterized by excellent reversibility in hydration/dehydration reactions [12–15].

MgH2, however, is not without its drawbacks. It has a high temperature of hydration/dehydration, a low rate of desorption/absorption of hydrogen due to thermodynamic stability ($\Delta H = 76$ kJ/mol) and slow kinetics (Ea = 160 kJ/mol) [16–20]. MgH2 is characterized by a strong metal-hydrogen bond energy, which gives a high thermal stability. These properties hinder the widespread practical application of MgH2 in various portable devices, in on-board fuel cells, such as those used in vehicles.

As a consequence, researchers face the challenge of improving the characteristics of storing hydrogen in materials.

Despite the thermodynamic barrier to reduce the dehydrogenation temperature of Mg-based materials [21], the Mg–H binding can be broken at room temperature. For example, in some compounds based on rare earth elements, in alloys based on Mg [20,22–25].

It was discovered [26] that MgH2, synthesized using H2 at a pressure of 30 atm in a ball mill with subsequent heat treatment and annealing has the desorption temperature (325 °C), kinetic dehydration (6.60 wt% in for 30 min at 300 °C and a hydrogen pressure of 20 atm), and also retains a capacity of more than 6.00 wt% (loss 0.60 wt%) after 10 hydration/dehydration cycles.

Transitional metals are promising catalysts for improving MgH2 hydrogen storage properties. However, obtaining uniformly dispersed and ultrafine catalysts based on transition metals with high catalytic activity is also problematic [15]. Despite the fact that various approaches have been proposed to address these problems, such as doping [27–30], nanostructuring of powder particles [31], research into the practical application of MgH2 is still in progress [32,33].

Another problem along this path is the need to use hydrogen beyond high purity, without any impurities. This is due to the effect of poisoning the electrodes of fuel cells with impurities.

Creation of materials based on particles with a core-shell structure, in the case when the shell is permeable only for hydrogen will solve this problem. In addition, using a transient metal of the platinum group as a shell can also reduce the energy of energy barriers.

Indeed, the Pd crystalline grid allows hydrogen ions to pass through, but remains impermeable to other gases, thereby purifying the gas from impurities. The idea of creating nanoballons on the basis of such materials was put forward at the beginning of this century, but it remains unresolved to date [34,35].

A group of researchers obtained platinum nanoparticles fixed on reduced graphite oxide to use as hydrogenation catalysts [36]. Palladium is also used. It has excellent catalytic activity for both hydrogen oxidation and oxygen reduction [37].

The properties of hydride materials can be adapted tailored to meet the stated goals for practical work, but this is highly dependent on the earliest stages of the synthetic approaches used and their effectiveness in achieving the desired characteristics.

The role of the carbon coating is that due to the developed surface (a large number of pores, their size), they demonstrate excellent adsorption and absorption properties [38], the

Please cite this article as: Churilov GN et al., Obtaining particles with the structure Mg@C and (Mg@C)@Pd, their properties and stability in the hydrogenation/dehydrogenation processes, International Journal of Hydrogen Energy, https://doi.org/10.1016/j.ijhydene.2021.03.042

presence of which is important for hydrogen storage [39]. It is known that pores with molecular sizes can absorb large amounts of gases due to the increased density of the adsorbed material inside the pores [40]. This is a consequence of the attractive potential of the pore walls. In addition, both chemical and plasma-chemical methods can apply a decorated shell of palladium to the surface of magnesium particles. Therefore, in this work, carbon was preliminarily deposited on magnesium particles, which made it possible to obtain a continuous palladium shell. Thanks to our approach to the creation of a nanostructured palladium catalyst, the specific surface area of particles and materials from them increase significantly.

This article presents a new approach to creating a nanostructured palladium catalyst. It consists in the application of a special technique for obtaining powders with particles (Mg@C)@Pd having a double dense shell. These particles are characterized by a lower hydration/dehydration temperature, increased resistance to recycling, no need for ultra-clean hydrogen, and a high sorbation capacity.

The catalytic properties of the obtained (Mg@C)@Pd improve the parameters of MgH2 hydrogen storage.

Materials and methods

The initial Mg - Sample 1 (S1) powder, which we obtained is studied in this work as a possible hydrogen accumulator and also as a core for particles, the core-shell Mg@C and (Mg@C)@Pd was synthesized in an arc discharge plasma of low frequency (LF). The low-frequency arc discharge was carried out in a chamber in an atmosphere of argon with small impurities of hydrogen (2–3 at.%) and nitrogen (8–9 at.%) between the tungsten electrode and the magnesium melt. An LF generator was used as a power source for the discharges used in this work. All syntheses were performed at a frequency of 66 kHz.

The morphology, size and structure of particles were observed by a SEM Hitachi S-5500 scanning electron microscope (SEM). Fig. 1 shows a scanning electron microscopic (SEM) image of a magnesium sample - S1.

It can be seen that the resulting Mg nanoparticles are irregularly shaped and agglomerated. On average, the size of the agglomerates reaches 100, and the particle size - several tens of nanometers.

To obtain powders with a core-shell particle structure, a specially designed setup was applied, the circuit diagram of which is shown in Fig. 2. The discharge was carried out in a stream of argon-forming plasma between two electrodes, one of which is replaceable. The installed electrode can be both a metal one, cooled by water, or a graphite. The discharge was stabilized by a vortex flow of nitrogen gas with an admixture of hydrogen, and an axial low-frequency magnetic field, which was in phase with the low-frequency current of the discharge.

The installation includes a water-cooled chamber, in the lower part of which there is a plasma generator with a replaceable metal or graphite electrode and a coil that creates a stabilizing magnetic field. In the upper part of the chamber, which performs the function of a quenching device, there is a second electrode made of water-cooled copper tube.

The paper [39] presents the study results of the carbon nanostructures as hydrogen sorbents (fullerenes, nanotubes, nanofibers, graphene structures), metal-carbon composites. It is shown that the MgH2–C systems can be used for the production of hydrogen accumulators of repeated action.

The powders with the Mg@C - Sample 2 (S2) structure were synthesized using a graphite rod with a diameter of 6 mm and an axial hole with a diameter of 3 mm. Magnesium particles were fed through an axial hole with a stream of argon. Nitrogen with a small admixture of hydrogen (2–3 at.%) was used as a vortex stabilizing flow.

Fig. 3 shows an SEM image of the particles of the resulting powder. The characteristic particle size is 50–70 nm. S2 particles have a clearly defined crystal faceting corresponding to hexagonal structures (Fig. 3 a). An amorphous carbon layer can also be observed on the surface of the Mg particles.

Palladium protects the sample from oxidation and accelerates hydrogen decomposition reactions. The synthesis of powders with particles (Mg@C)@Pd was carried out on a setup (Fig. 2) with a palladium electrode. The amount of palladium in the plasma stream generated during the erosion of the electrode was insufficient, and therefore only a few percent of the powder with particles (Mg@C)@Pd was obtained. This amount was not enough for research. To solve this problem,

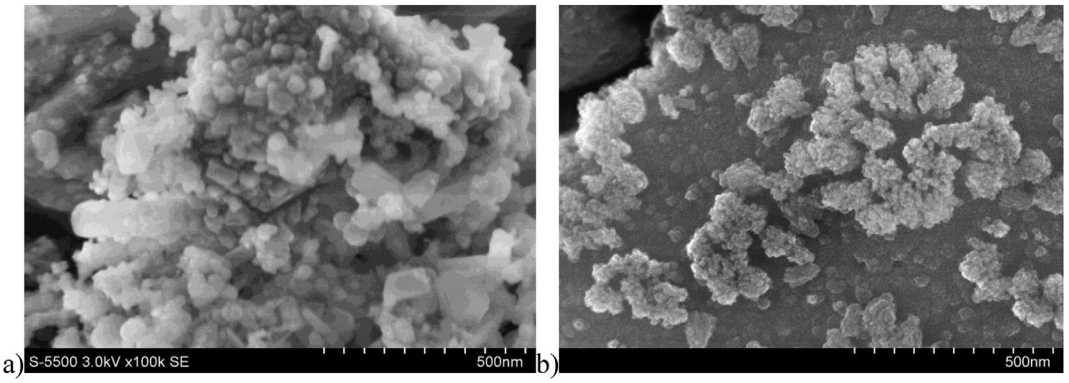

Fig. 1 – SEM image of S1: a) before hydrogenation, b) after 10 cycles of hydrogenation/dehydrogenation.

Please cite this article as: Churilov GN et al., Obtaining particles with the structure Mg@C and (Mg@C)@Pd, their properties and stability in the hydrogenation/dehydrogenation processes, International Journal of Hydrogen Energy, https://doi.org/10.1016/j.ijhydene.2021.03.042

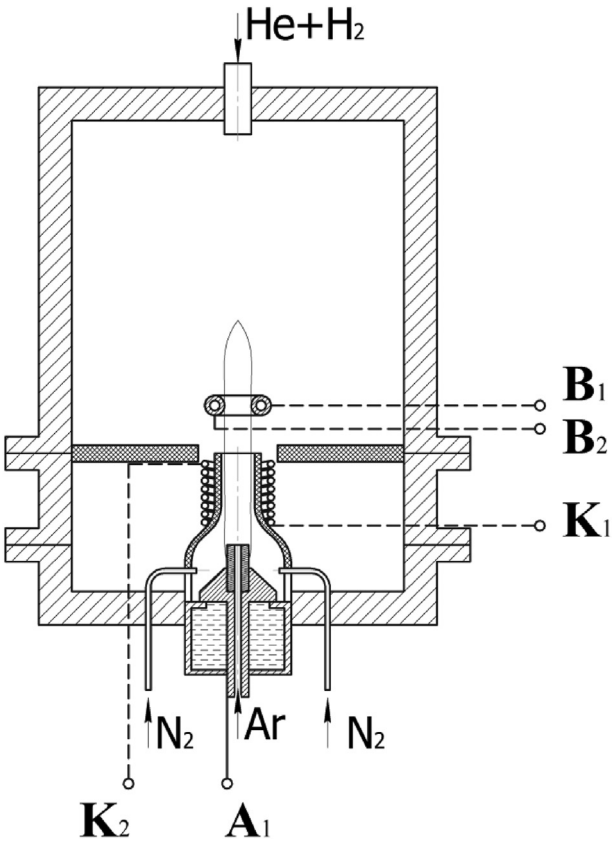

Fig. 2 – Scheme of a plasma-chemical installation based on a plasma generator with magnetic and vortex stabilization with a replaceable electrode.

we developed a technique that allows to increase the palladium content in the reaction zone (i.e., in the discharge gap). The technique is based on the interaction of a thermally unstable organometallic complex - palladium (II) acetylacetonate [Pd (C5H7O2) 2] with hot Mg@C particles transported by the plasma stream.

The process is schematically presented in Fig. 4.

The figure illustrates how particles of the core material enter plasma stream with plasma-forming gas stream (1) rotating at ω1 frequency. Then, under the action of centrifugal force, they fall into the stream of stabilizing vortex gas (2), which is transported for palladium acetylacetonate and has a rotation frequency of ω2 (greater than ω1). Palladium (II) acetylacetonate molecules [Pd (C5H7O2) 2], with decomposition temperature equals to 478 K, colliding with hot Mg@C particles, fell apart, leaving palladium on their surface (in Fig. I, II and III). Both rotating streams, plasma and vortex stabilizing, fall into the upper part of the chamber, which acts as a quenching device, where light and heavy components are separated due to the centrifugal force. The light particles move slowly from the axis of rotation to the wall, while the heavy ones move quickly. There is a translational movement of the gas flow along the axis, so heavy particles settle on the bottom of the chamber, and light particles get to the top. As it turns out, the particle condensate in the lower part of the chamber consists of more than 90 wt% of (Mg@C)@Pd particles.

The particles of the isolated powder (Mg@C)@Pd - Sample 3 (S3) have a mostly pronounced spherical shape. In the photographs, two types of particles can be distinguished: small and large. It can be seen that the particle size (Mg@C)@Pd is mainly 20–100 nm. The average particle size is about 90 nm, which is larger than Mg@C. However, there are larger particles, reaching several hundred nanometers. The particles do not agglomerate. The SEM image is shown in Fig. 5.

The results of analytical studies of samples during hydrogenation/dehydrogenation

The study was conducted using hydrogen (99.995 wt%) in the following sequence. S1, S2 and S3 were alternately placed in the cell of a specially manufactured installation for studying hydrogenation/dehydrogenation processes. The cell was vacuumed and kept at a temperature of 120 °C for 10 min, then hydrogen was introduced into it. Hydrogen sorption was carried out at the initial pressure of 100 bar. For S1, the hydrogenation temperature was subsequently: 430°C, for S2 - 400°C, for S3 - 380°C. Desorption occurred due to heating of the samples to the following temperature levels: for S1 - 500°C, for S2 - 450°C, for S3 - 400°C. For each sample, the hydrogenation/dehydrogenation process was repeated during 10 cycles.

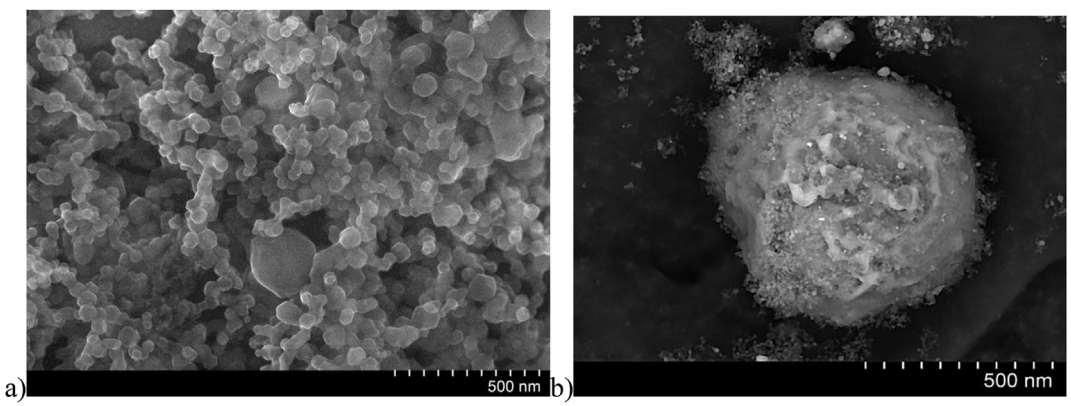

Fig. 3 – SEM image S2: a) before hydrogenation, b) after 10 cycles of hydrogenation/dehydrogenation.

Please cite this article as: Churilov GN et al., Obtaining particles with the structure Mg@C and (Mg@C)@Pd, their properties and stability in the hydrogenation/dehydrogenation processes, International Journal of Hydrogen Energy, https://doi.org/10.1016/j.ijhydene.2021.03.042

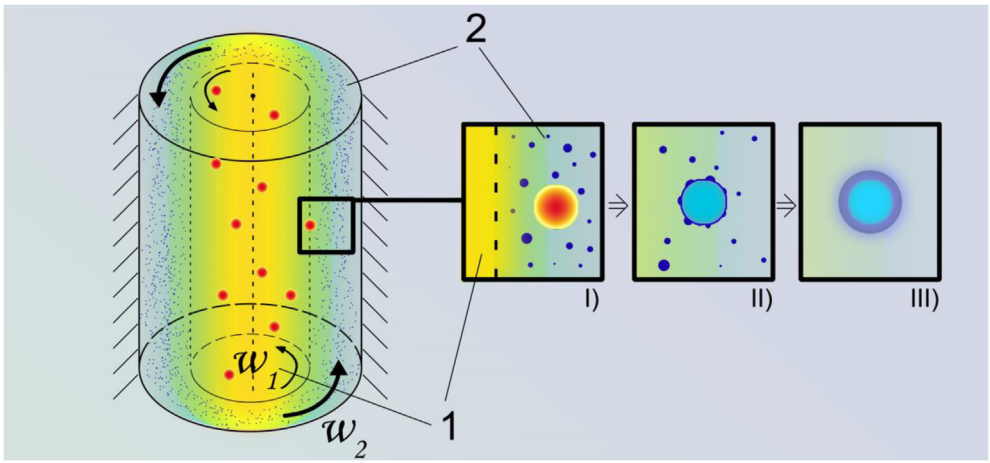

Fig. 4 – Schematic description of the synthesis technique of core-shell particles using thermally unstable organometallic complexes.

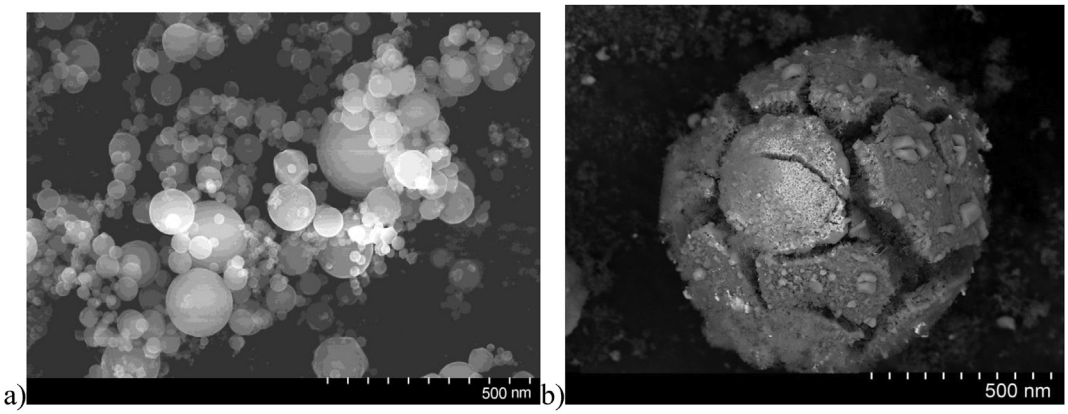

Fig. 5 – SEM image of S3: a) before hydrogenation, b) after 10 cycles of hydrogenation/dehydrogenation.

There was no contact with the environment between the cycles. Before each cycle, each sample was cooled to room temperature. Immediately after the synthesis, the obtained samples were containing 0.1–0.2 wt% of hydrogen, thus, justifying a zero dehydrogenation cycle carried out prior to the cyclic reactions.

The amount of hydrogen released was determined by the change in pressure, which was measured by a pressure sensor.

Weight percentage conversion was calculated in accordance with the obtained dependences of pressure and time.

Sample 1 (S1)

Fig. 6 shows a graph of the change in the weight content of hydrogen over 10 cycles of hydrogenation/dehydrogenation.

The maximum hydrogen content was equal to 4.65 wt%. In case of sequential cyclic implementation of the hydrogenation/dehydrogenation reaction, the sorption capacity started to decrease after the 3rd cycle.

To study the characteristics of the obtained powders, the X-ray photoelectron spectroscopy (XPS) method was used, which is based on measuring the energy of photoelectrons knocked out from various energy levels of atoms when a substance is irradiated with X-rays. An ultrahigh vacuum photoelectron spectrometer UNI-SPECS spectrometer, manufactured by SPECS Gmbh, was used. In the course of the study, the surface of the sample was cleaned by the method of etching the surface with argon ions: for 1 min, the surface of the sample was treated with argon ions with an energy of 1 kW, which led to the evaporation of the upper layer.

Fig. 7 shows XPS spectra for S1 before and after hydrogenation, and after the fall of the capacity. Immediately after the synthesis in the S1 line of the Mg2p binding energy of 49.2 eV corresponds to the concentration 86.21 at.% of magnesium metal, and the hydride and magnesium oxide accounts for 8.62 at.% and 5.17 at.%, respectively.

The presence of magnesium hydride after the preliminary cycle of desorption facilitates hydrogenation, creating paths and gaps in the layer of magnesium oxide on the surface of the particles. This is confirmed by the fact that hydrogenation is not finished. Fig. 7 c shows the line Mg2s XPS spectrum for the sample after hydrogenation to maximum capacity. After conducting a mathematical decomposition of the spectrum in terms of bands, it was determined that magnesium hydride in

Please cite this article as: Churilov GN et al., Obtaining particles with the structure Mg@C and (Mg@C)@Pd, their properties and stability in the hydrogenation/dehydrogenation processes, International Journal of Hydrogen Energy, https://doi.org/10.1016/j.ijhydene.2021.03.042

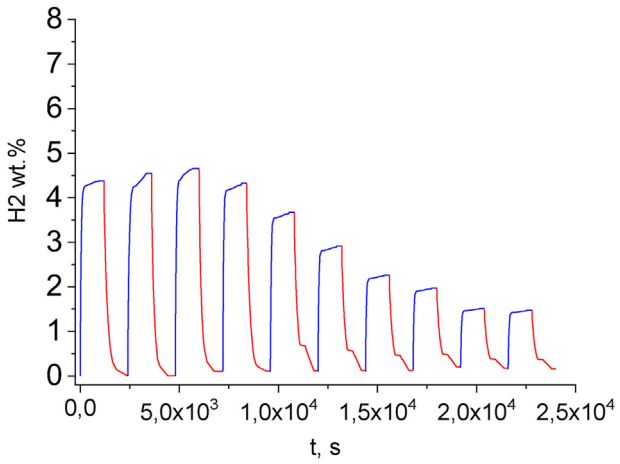

Fig. 6 – Graph of the weight content of hydrogen in S1. The growth curve of the weight content of hydrogen during hydrogenation is colored blue, and the curve of the decrease in weight content of hydrogen during dehydrogenation is red. (For interpretation of the references to color in this figure legend, the reader is referred to the Web version of this article.)

the sample equals to – 67.95 at.%. at the same time on a metal magnesium and magnesium oxide and have 14.15 at.%, 17.90 at.%, respectively.

Analyzing the line O1s XPS spectrum (Fig. 7 b and d) we can observe that for the initial sample 95.80 at.% oxygen in the sample corresponds to MgO. After the fall of the capacity absorbed by the sample, the oxygen is distributed between MgO and Mg(OH)2 (531.73 and 529.98 eV) with the concentration 46.26 at.% and 53.74 at.%, respectively.

Thus, the decrease in sorption capacity of magnesium is due to the formation of oxides and hydroxides of magnesium. The obtained data provide evidence proving that in order to use hydrogen of technical level purity it is essential to apply particles, protected by a sheath, for example of carbon. Our assumption was confirmed in the works [41,42]. The authors point out that the main disadvantage of MgH2 as hydrogen storage is the high reactivity to air and oxygen.

Sample 2 (S2)

The above described method S2, containing particles of Mg@C, was investigated as a hydrogen battery. Tests were performed in the sorption capacity of S2. The hydrogenation was carried out at a temperature of 400 °C and under pressure of 100 bar. The reaction of dehydrogenation was carried out by heating up to 450 °C with atmospheric pressure of hydrogen in the measurement cell.

Fig. 8 shows a graph of the weight change of hydrogen content in S2 during 10-fold cyclic hydrogenation/dehydrogenation.

At the beginning of the hydrogen absorption process, H2 molecules can easily pass through the thin carbon layer. The maximum sorption capacity of the sample for hydrogen – 5.12 wt% is reached in the second cycle. As presented in Fig. 8, after the 3rd sorption cycle, the sample does not completely release the absorbed hydrogen. At the same time, with further hydrogenation, an increase in the weight of absorbed hydrogen is detected, and the released one remains at the same level, inclusively along the 7th cycle. The XRD spectrum shows that after hydrogenation of S2, the amorphous halo intensifies and the relative intensity of the MgO phase reflections increases.

Fig. 9 shows XPS spectra for S2 before and after hydrogenation. Immediately after the synthesis in the S2 line Mg2p binding energy 49.85 eV corresponds to the concentration 80.72 at.% metallic magnesium, when 54.83 eV peak corresponds to the connection of carbon and magnesium with concentration of 11.73 at.%. After etching the magnesium concentration increases to 95.54 at.%, and the number of magnesium atoms associated with the carbon is reduced to 4.46 at.%. Therefore, the relationship of carbon with magnesium is carried out near the surface of particles and corresponds to the interface layer between the core and shell of the MgC.

Analysis of the C1s line for S2 shows the presence of carbon in sp2 and sp3 hybridization ratio of 62.81 and 28.42 at.%, respectively. Mathematical decomposition of the band helped to identify the peaks corresponding to the Mg–C binding energy 281.15 eV and a concentration of 3.42 at.%, and the band that corresponds to the relations groups C-O/C=O with binding energy 289.2 eV and a concentration of 5.35 at.%.

After the hydrogenation along the Mg2s S2 line the presence of peaks corresponding MgH2, Mg and MgO with concentrations 56.56 at.%, 40.56 at.% and 2.88 at.% can be respectively observed. At the same time, the proportion of atoms of magnesium metal with the increase of cycles decreases and the proportion of the hydride increases. After the 3rd cycle concentration of MgH2 and Mg show the indication of 85.35 at.% and 12.21 at.%, after 7-its a cycle – 95.30 and 2.13 at.%, respectively.

Line C1s after hydrogenation 60.05 at.% accounts for the sp2-hybridization of carbon and 22.09 at.% in sp3 hybridization, while, on the connection of Mg–C accounts for 1.96 at.%, and group C–O/C=O 15.90 at.%. After etching by argon ions on sp2-hybidization has 74.22 at.%, for sp3-hybridization – 8.56 at.%, for the Mg–C concentration corresponds to 4.78 at.%, and the group C–O/C=O – 8.83 at.%. In addition, the energy peak of 287.55 eV was detected in the process of decomposition, which corresponds to the group C–O/O–H with a concentration of 3.60 at.%.

At the zero cycle of dehydrogenation channels for the release of hydrogen are formed. The hydrogen diffuses through the carbon shell, finding new channels of penetration inside the kernel of magnesium, thus, accumulating in the interface layer and reducing the contact phase of Mg–C. As a result, each cycle of hydrogenation/dehydrogenation S2 retains the hydrogen, with the following cycle taking more hydrogen due to the higher completion of hydrogenation of magnesium. In this case, carbon shell prevents impurities of oxygen and water, accumulating defects of the structure. After the defects of shell exceed a certain critical value, the process of carbon shell degradation occurs under the action of hydrogen resulting with the formation of oxides and hydroxides and the carbonyl groups (C–O–H), which can be observed as a sharp drop in the sorption capacity from cycle 8 to 10. Fig. 3 b shows the image of particle

Please cite this article as: Churilov GN et al., Obtaining particles with the structure Mg@C and (Mg@C)@Pd, their properties and stability in the hydrogenation/dehydrogenation processes, International Journal of Hydrogen Energy, https://doi.org/10.1016/j.ijhydene.2021.03.042

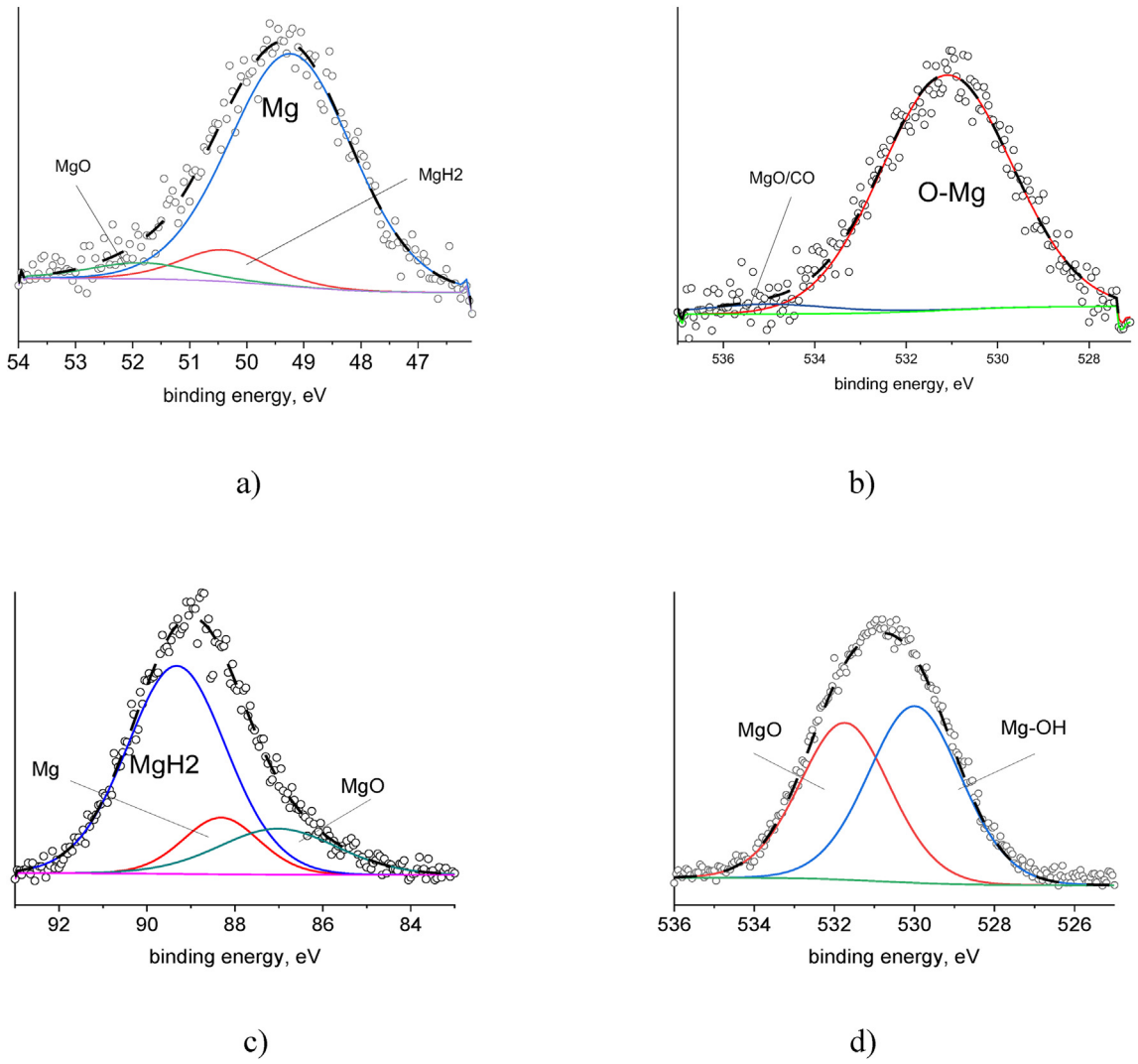

Fig. 7 – XPS for S1: a) Mg2p line before hydrogenation; b) line O1s before hydrogenation, c) line of magnesium Mg2s after hydrogenation, d) line O1s after 10 cycles of hydrogenation/dehydrogenation.

S2 after the capacity decrease, highlighting the morphology differing from the original sample with the bigger amount of shell defects.

Sample 3 (S3)

To prevent "poisoning" of the carbon shell by the impurities of oxygen and water vapor, and also to reduce the activation barrier of hydrogenation, S3 sample was synthesized, as powder with particles (Mg@C)@Pd. Additional palladium shell acts as a micro- or nanoballon. Palladium is a noble metal which lattice is capable of passing hydrogen. Moreover, surface defects of the palladium crystal lattice have a positive catalytic effect for the dissociation of hydrogen molecules, which facilitates its diffusion [43,44]. The main advantage of the method applied for producing S3 particles is the restoration of the oxide layer of magnesium particles during the deposition of a carbon shell with the subsequent application of a protective palladium shell on it. Both carbon and palladium in the form of continuous shells are impermeable to oxygen and water vapor, however, they have the ability of bulk diffusion of hydrogen [45,46]. In this case, the inevitably occurring oxides of the protective shell can be easily removed in the form of CO and CO2 when heated to temperatures of 100–120 °C.

Fig. 10 shows a graph illustrating the change in the weight content of hydrogen in S3 at 10-fold cyclic hydrogenation/dehydrogenation.

During the cyclic hydrogenation of S3, the maximum sorption capacity is observed already after the first cycle, which is 6.94 wt% and remains constant until the 5th cycle, after which it begins to decrease. XRD was performed before and after hydrogenation. As a result of hydrogenation, the phases Pd, Mg, MgH2, MgO were detected in S3, and a 23.6° reflex identified as a reflection from graphite planes was also observed. After the 10th dehydrogenation cycle, amplification of MgO and an additional phase of Mg (OH) 2 are observed in the sample.

Please cite this article as: Churilov GN et al., Obtaining particles with the structure Mg@C and (Mg@C)@Pd, their properties and stability in the hydrogenation/dehydrogenation processes, International Journal of Hydrogen Energy, https://doi.org/10.1016/j.ijhydene.2021.03.042

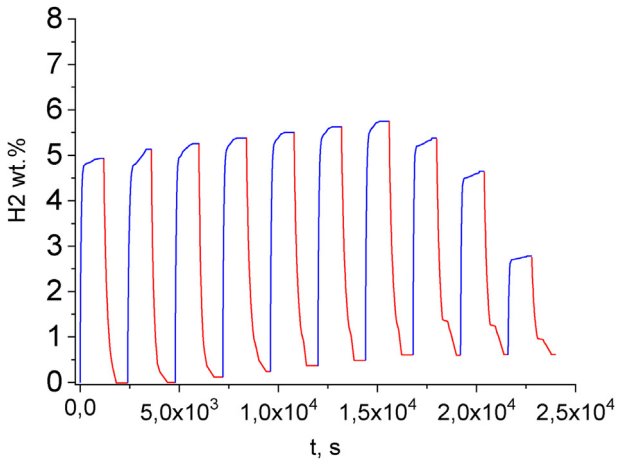

Fig. 8 – Graph of the weight content of hydrogen in S2. The growth curve of the weight content of hydrogen during hydrogenation is marked in blue; the curve for the decrease in weight content of hydrogen during dehydrogenation is red. (For interpretation of the references to color in this figure legend, the reader is referred to the Web version of this article.)

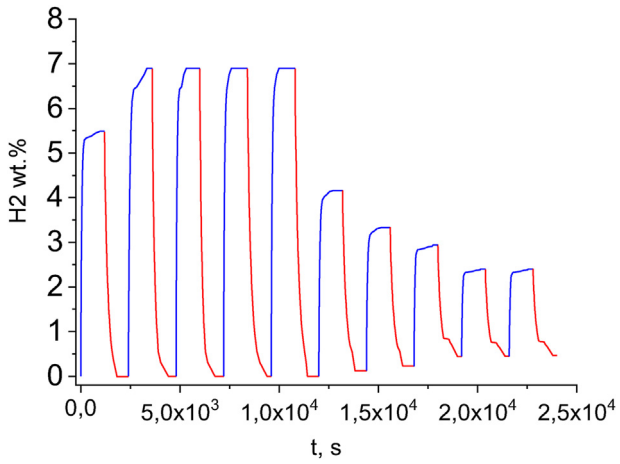

Fig. 10 – Graph of the weight content of hydrogen in S3. The growth curve of the weight content of hydrogen during hydrogenation is colored blue; the curve of the fall of the weight content of hydrogen during dehydrogenation is red. (For interpretation of the references to color in this figure legend, the reader is referred to the Web version of this article.)

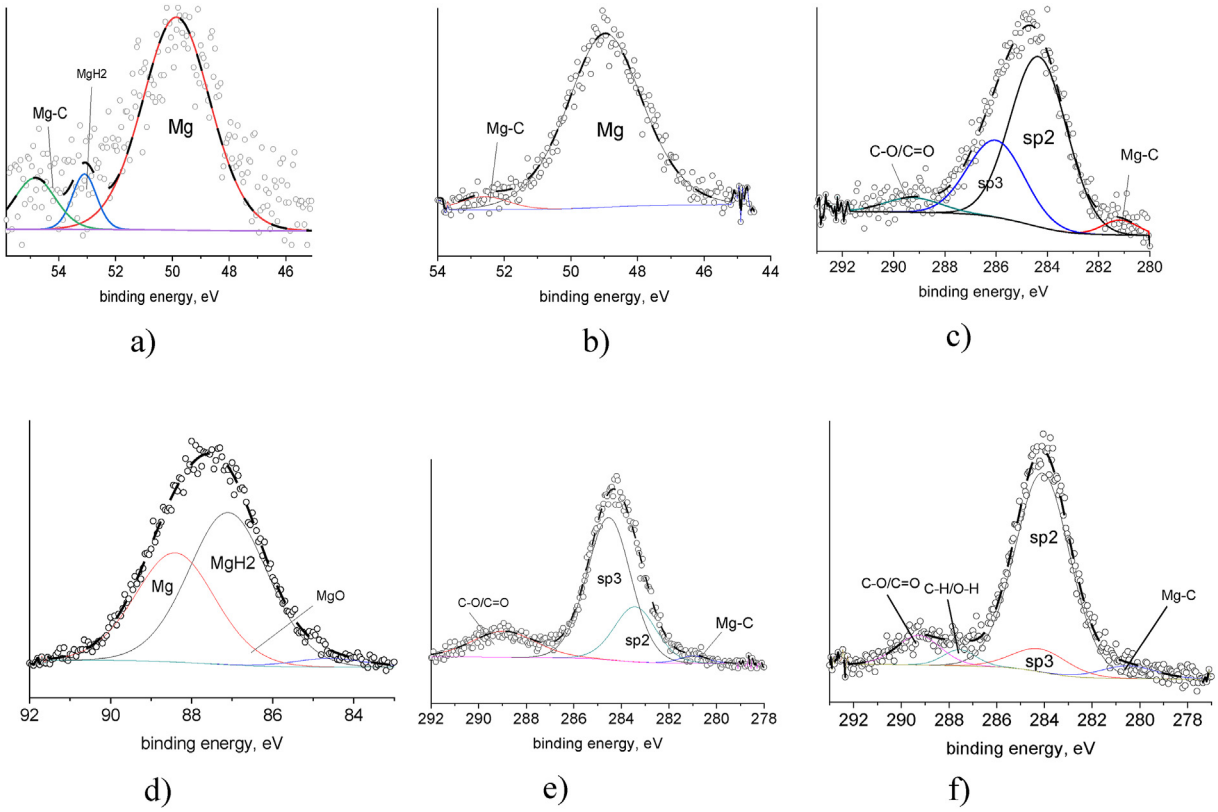

Fig. 9 – XPS S2: a) Mg2p line before sample hydrogenation, b) the Mg2p line after etching of the surface with argon ions, c) line C1s before hydrogenation, d) line Mg2s after hydrogenation, e) the C1s line after hydrogenation; f) the C1s line of the hydrogenated sample after etching the surface with argon ions.

The composition of S3 particles was conducted with the use of XPS method. The results are presented in Fig. 11.

According to microscopy and XPS composition (wt.%): (Mg@C)@Pd (92:2:6).

Mathematical decomposition of the Mg2s line shows the presence of peaks of Mg, MgO, and Mg(OH)2 with concentrations of 81.58 at.%, 6.94 at.% and 11.48 at.%, respectively. There is a doublet of lines along the Pd3d3/2 line, the mathematical

Please cite this article as: Churilov GN et al., Obtaining particles with the structure Mg@C and (Mg@C)@Pd, their properties and stability in the hydrogenation/dehydrogenation processes, International Journal of Hydrogen Energy, https://doi.org/10.1016/j.ijhydene.2021.03.042

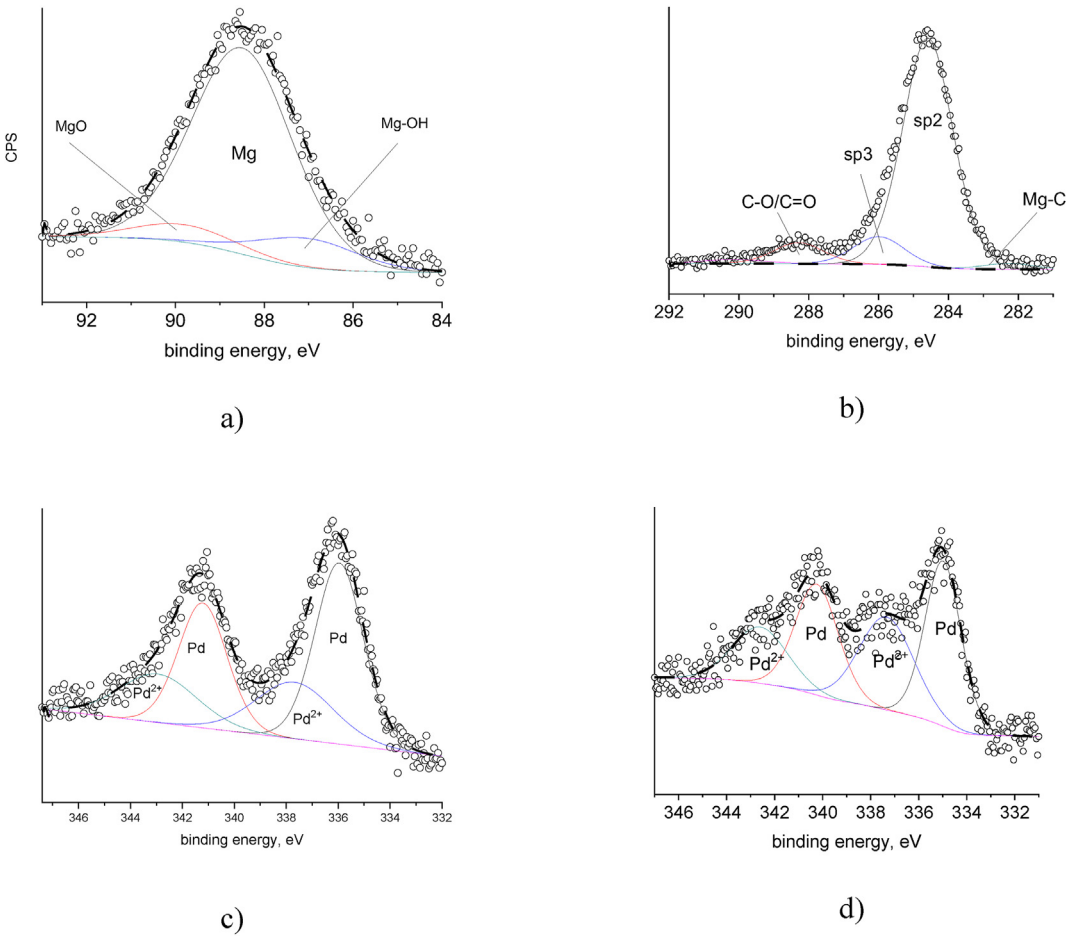

Fig. 11 – XPS S3: a) Mg2s line before hydrogenation, b) line C1s before hydrogenation, c) line Pd3d3/2 before hydrogenation, d) Pd3d3/2 line before hydrogenation after etching with argon ions.

decomposition of which shows the presence of Pd0 and Pd2+ with concentrations of 64.74 and 35.27 at.%, respectively. The binding energy of 337.34 eV indicates an increase in the concentration of Pd2+ atoms upon etching of the sample. This suggests that chemically bonded palladium atoms have a higher concentration approaching the nucleus of the particle.

Similarly, as in S2, after the zero-desorption cycle, hydrogen forms channels for movement through the Mg@C interface layer. Further, as a result of sequential hydrogenation/dehydrogenation, the contact phase decreases and defects in the carbon layer accumulate, which, in turn, leads to the destruction of the palladium shell. As a result of the destruction of the protective shell, the water and oxygen impurities accumulated by the sample have a "poisonous" effect on S3, leading to a sharp decrease in the sorption capacity.

Fig. 5 b shows the image of the particle S3 after a drop in the capacitance. Cracks are observed on the particle surface, which confirms the above considerations. The accumulation of defects in the interface layers of S3 particles leads to a violation of the integrity of the protective coating of the magnesium core, after which its sorption capacity decreases sharply.

Conclusion

In the course of the suggested studies, it was found that when using hydrogen (99.995 wt%), the resistance of powders containing nanosized particles of Mg, Mg@C and (Mg@C)@Pd to cyclic hydrogenation/dehydrogenation decreases as a result of the accumulation of MgO and $Mg(OH)_2$. Coating magnesium particles with a carbon shell increases the sorption capacity and resistance to cyclic hydrogenation/dehydrogenation. However, under the influence of "poisonous" factors, the carbon shell is destroyed. Particles with two shells, carbon and palladium, i.e. with the structure (Mg@C)@Pd are characterized by the increased stability, up to 5 hydrogenation/dehydrogenation cycles, a significant amount of stored hydrogen - 6.95 wt %, as well as a decrease in the temperature of hydrogen sorption to 380 °C and desorption to 400 °C.

In accordance with the results obtained for the accumulation of hydrogen with a purity of 99.995 wt%, the use of powders with particles having the structure (Mg@C)@Pd leads to a positive effect. However, a high content of particles with a

Please cite this article as: Churilov GN et al., Obtaining particles with the structure Mg@C and (Mg@C)@Pd, their properties and stability in the hydrogenation/dehydrogenation processes, International Journal of Hydrogen Energy, https://doi.org/10.1016/j.ijhydene.2021.03.042

continuous palladium shell is not enough to obtain a material with a high degree of resistance to the cyclic hydrogenation/dehydrogenation process. Particles of large size (several hundred nm) are destroyed first. Thus, further work should be related to the study of the influence of the size effect of particles on their mechanical resistance to the cyclic hydrogenation/dehydrogenation process.

Declaration of competing interest

The authors declare that they have no known competing financial interests or personal relationships that could have appeared to influence the work reported in this paper.

Acknowledgements

This work was supported by and carried out on the equipment of the Center for Common Use of the Krasnoyarsk Scientific Center, Siberian Branch, Russian Academy of Sciences.

REFERENCES

[1] Schlapbach L, Züttel A. Hydrogen-storage materials for mobile applications. Nature 2001;414:353–8. https://doi.org/10.4236/ns.2010.21003.
[2] Felderhoff M, Weidenthaler C, von Helmolt R, Eberle U. Hydrogen storage: the remaining scientific and technological challenges. Phys Chem Chem Phys 2007;9:2643–53. https://doi.org/10.1039/b701563c.
[3] Andersson J, Grönkvist S. Large-scale storage of hydrogen. Int J Hydrogen Energy 2019;44(23):11901–19. https://doi.org/10.1016/j.ijhydene.2019.03.063.
[4] Sakintuna B, Lamaridarkrim F, Hirscher M. Metal hydride materials for solid hydrogen storage: a review. Int J Hydrogen Energy 2007;32:1121–40. https://doi.org/10.1016/j.ijhydene.2006.11.022.
[5] Lim KL, Kazemian H, Yaakob Z, Daud WRW. Solid-state materials and methods for hydrogen storage: a critical review. Chem Eng Technol 2010;33:213–26. https://doi.org/10.1002/ceat.200900376.
[6] Renju Z, ullah S. Rather Review of solid state hydrogen storage methods adopting different kinds of novel materials. J Nanomater 2015;2015:1–18. https://doi.org/10.1155/2015/914845.
[7] Chen P, Zhu M. Recent progress in hydrogen storage. Mater Today 2008;11:36–43. https://doi.org/10.1016/S1369-7021(08)70251-7.
[8] Lai Q, Paskevicius M, Sheppard DA, Buckley CE, Thornton AW, Hill MR, et al. Hydrogen storage materials for mobile and stationary applications: current state of the art. ChemSusChem 2015;8:2789–825. https://doi.org/10.1002/cssc.201500231.
[9] Graetz J. New approaches to hydrogen storage. Chem Soc Rev 2009;38:73–82. https://doi.org/10.1039/b718842k.
[10] Eberle U, Felderhoff M, Schüth F. Chemical and physical solutions for hydrogen storage. Angew Chem Int Ed 2009;48:6608–30. https://doi.org/10.1002/anie.200806293.
[11] Van den Berg AWC, Areán CO. Materials for hydrogen storage: current research trends and perspectives. Chem Commun 2008;6:668–81. https://doi.org/10.1039/B712576N.
[12] Huang Z, Guo Z, Calka A, Wexler D, Liu H. Improvement in hydrogen cycling properties of magnesium through added graphite. Mater Lett 2007;61:3163–6. https://doi.org/10.1016/j.matlet.2006.11.017.
[13] Huang Z, Guo Z, Calka A, Wexler D, Wu J, Notten PHL, et al. Noticeable improvement in the desorption temperature from graphite in rehydrogenated MgH2/graphite composite. Mater Sci Eng, A 2007;447:180–5. https://doi.org/10.1016/j.msea.2006.11.074.
[14] Gattia DM, Jangir M, Jain IP. Study on nanostructured MgH2 with Fe and its oxides for hydrogen storage applications. J Alloys Compd 2019;801:188–91. https://doi.org/10.1016/j.jallcom.2019.06.067.
[15] Meng Q, Huang Y, Ye J, Xia G, Wang G, Dong L, et al. Electrospun carbon nanofibers with in-situ encapsulated Ni nanoparticles as catalyst for enhanced hydrogen storage of MgH2. J Alloys Compd 2021;851:156874. https://doi.org/10.1016/j.jallcom.2020.156874.
[16] Peng B, Liang J, Tao Z, Chen J. Magnesium nanostructures for energy storage and conversion. J Mater Chem 2009;19:2877–83. https://doi.org/10.1039/B816478A.
[17] Cheng F, Tao Z, Liang J, Chen J. Efficient hydrogen storage with the combination of lightweight Mg/MgH2 and nanostructures. Chem Commun 2012;48:7334–43. https://doi.org/10.1039/c2cc30740e.
[18] Huang Z, Guo Z, Calka A, Wexler D, Liu H. Effects of carbon black, graphite and carbon nanotube additives on hydrogen storage properties of magnesium. J Alloys Compd 2007;427:94–100. https://doi.org/10.1016/j.jallcom.2006.03.069.
[19] Jain IP, Lal C, Jain A. Hydrogen storage in Mg: a most promising material. Int J Hydrogen Energy 2010;35:5133–44. https://doi.org/10.1016/j.ijhydene.2009.08.088.
[20] Fursikov PV, Tarasov BP. Hydrogen sorbing magnesium alloys and composites. Russ Chem Bull 2018;67(2):193–9.
[21] Dornheim M, Doppiu S, Barkhordarian G, Boesenberg U, Klassen T, Gutfleisch O, et al. Hydrogen storage in Mg-based hydrides and hydride composites. Scripta Mater 2007;56:841–6. https://doi.org/10.1016/j.scriptamat.2007.01.003.
[22] Zou J, Zeng X, Ying Y, Chen X, Guo H, Zhou S, et al. Study on the hydrogen storage properties of core–shell structured Mg–RE (RE = Nd, Gd, Er) nano-composites synthesized through arc plasma method. Int J Hydrogen Energy 2013;38(5):2337–46. https://doi.org/10.1016/j.ijhydene.2012.11.145.
[23] Zou J, Zeng X, Ying Y, Stephane P, Ding W. Preparation and hydrogen sorption properties of a nano-structured Mg based Mg–La–O composite. Int J Hydrogen Energy 2012;37(17):13067–73. https://doi.org/10.1016/j.ijhydene.2012.04.136.
[24] Li QA, Liu WC, Song XJ. Research progress of Mg-Re alloys. Adv Mater Res 2014;937:178–81. https://doi.org/10.4028/www.scientific.net/amr.937.178.
[25] Fursikov PV, Fattakhova AM, Mozhzhukhin SA, Blinova LN, Tarasov BP. Hydrogen containing composites of magnesium hydride with lanthanide oxides. Alternative Energy and Ecology (ISJAEE) 2017;1–3:34–45. https://doi.org/10.15518/isjaee.2017.01-03.034-045. In Russ.
[26] Bhatnagar A, Shaz MA, Srivastava ON. Synthesis of MgH2 using autocatalytic effect of MgH2. Int J Hydrogen Energy 2019;44(13):6738–47. https://doi.org/10.1016/j.ijhydene.2019.01.163.
[27] Ouyang LZ, Cao ZJ, Li LL, Wang H, Liu JW, Min D, et al. Enhanced high-rate discharge properties of La11.3Mg 6.0Sm7.4Ni61.0Co7.2Al7.1 with added graphene synthesized by plasma milling. Int J Hydrogen Energy 2014;39:12765–72. https://doi.org/10.1016/j.ijhydene.2014.06.111.

Please cite this article as: Churilov GN et al., Obtaining particles with the structure Mg@C and (Mg@C)@Pd, their properties and stability in the hydrogenation/dehydrogenation processes, International Journal of Hydrogen Energy, https://doi.org/10.1016/j.ijhydene.2021.03.042

[28] Čermák J, Král L. Hydrogen diffusion in Mg-H and Mg-Ni-H alloys. Acta Mater 2008;56:2677–86. https://doi.org/10.1016/j.actamat.2008.02.003.
[29] Janot R, Darok X, Rougier A, Aymard L, Nazri GA, Tarascon JM. Hydrogen sorption properties for surface treated MgH2 and Mg2Ni alloys. J Alloys Compd 2005;404–406:293–6. https://doi.org/10.1016/j.jallcom.2005.01.129.
[30] Chen M, Hu M, Xie X, Liu T. High loading nanoconfinement of V-decorated Mg with 1 nm carbon shells: hydrogen storage properties and catalytic mechanism. Nanoscale 2019;11:10045–55. https://doi.org/10.1039/C8NR09909J.
[31] Sun YH, Shen CQ, Lai QW, Liu W, Wang D-W, Aguey-Zinsou K-F. Tailoring magnesium based materials for hydrogen storage through synthesis: current state of the art. Energy Storage Mater 2018;10:168–98. https://doi.org/10.1016/j.ensm.2017.01.010.
[32] Shao H, Xin G, Zheng J, Li X, Akiba E. Nanotechnology in Mg-based materials for hydrogen storage. Nanomater Energy 2012;1(4):590–601. https://doi.org/10.1016/j.nanoen.2012.05.005.
[33] Edalati K, Uehiro R, Ikeda Y, Li H-W, Emami H, Filinchuk Y, et al. Design and synthesis of a magnesium alloy for room temperature hydrogen storage. Acta Mater 2018;149:88–96. https://doi.org/10.1016/j.actamat.2018.02.033.
[34] Churilov GN. Sinthesis and characterization of novel nanomaterials for hydrogen adsorption. In: The proceedings for the 38th ISTC Japan workshop on advanced technologies in Russia; 2006. p. 173–93. https://doi.org/10.1007/978-94-007-0899-0_14. Japan (Sendai-shi, Miyagi).
[35] Churilov GN, Osipova IV, Novikov PV, Grebennikova NV, Chesnokov NV. Hydrogenation and properties of Pd-Mg-C and Pd-Al-C nanodispersion systems. In: Proceedings of XI international conference «hydrogen materials science and chemistry of carbon nanomaterials» yalta; August 25-31 2009. p. 268–71. https://doi.org/10.13140/RG.2.2.27717.19688.
[36] Kushch SD, Kuyunko NS, Muradyan VE, Korshunova LA, Dremova NN, Tarasov BP. Platinum nanoparticles attached to reduced graphite oxide as hydrogenation catalysts. Alternative Energy and Ecology (ISJAEE) 2012;8(112):71–6 [In Russ.].
[37] Mougenot M, Caillard A, Brault P, Baranton S, Coutanceau C. High Performance plasma sputtered PdPt fuel cell electrodes with ultra low loading. Int J Hydrogen Energy 2011;36(14):8429–34.
[38] Elesina VI, Churilov GN, Vnukova NG, Dudnik AI, Osipova IV. Filtration process combined with mechanical action, as a method for efficient extraction of endohedral metallofullerenes from carbon soot. Fuller, Nanotub Carbon Nanostruct 2019;27(10):803–7. https://doi.org/10.1080/1536383X.2019.1648439.
[39] Tarasov BP, Muradyan VE, Volodin Synthesis AA. properties, and examples of the use of carbon nanomaterials. Russ.Chem.Bull., Int.Ed. 2011;60(7):1261–73.
[40] Dillon AC, Jones KM, Bekkedahl TA, Kiang CH, Bethune DS, Heben MJ. Storage of hydrogen in single-walled carbon nanotubes. Nature 1997;386:377–9. https://doi.org/10.1038/386377a0.
[41] Zaluska A, Zaluski L, Ström-Olsen JO. Nanocrystalline magnesium for hydrogen storage. J Alloys Compd 1999;288:217–25.
[42] Barkhordarian G, Klassen T, Bormann R. Effect of Nb2O5 content on hydrogen reaction kinetics of Mg. J Alloys Compd 2004;364:242–6.
[43] Ahmed F, Nagumo R, Miura R, Ai S, Tsuboi H, Hatakeyama N, et al. A. Miyamoto Comparison of reactivity on step and terrace sites of Pd (332) surface for the dissociative adsorption of hydrogen: a quantum chemical molecular dynamics study. Appl Surf Sci 2011;257(24):10503–13. https://doi.org/10.1016/j.apsusc.2011.07.028.
[44] Ahmed F, Alam MdK, Miura R, Suzuki A, Tsuboi H, Hatakeyama N, et al. Modeling of hydrogen vacancy for dissociative adsorption of H2 on Pd (111) surface by a quantum chemical molecular dynamics. Catal Today 2011;164(1):16–22. https://doi.org/10.1016/j.cattod.2010.10.009.
[45] Cheng H, Chen G, Zhang Y, Zhu Y, Li L. Boosting low-temperature de/re-hydrogenation performances of MgH2 with Pd-Ni bimetallic nanoparticles supported by mesoporous carbon. Int J Hydrogen Energy 2019;44(21):10777–87. https://doi.org/10.1016/j.ijhydene.2019.02.218.
[46] Pei P, Whitwick MB, Kureshi S, Cannon M, Quan G, Kjeang E. Hydrogen storage mechanism in transition metal decorated graphene oxide: the symbiotic effect of oxygen groups and high layer spacing. Int J Hydrogen Energy 2020;45(11):6713–26. https://doi.org/10.1016/j.ijhydene.2019.12.095.

Please cite this article as: Churilov GN et al., Obtaining particles with the structure Mg@C and (Mg@C)@Pd, their properties and stability in the hydrogenation/dehydrogenation processes, International Journal of Hydrogen Energy, https://doi.org/10.1016/j.ijhydene.2021.03.042